Acta Cryst. (1993). D**49**, 381–388

Structure of the Mammalian Catalytic Subunit of cAMP-Dependent Protein Kinase and an Inhibitor Peptide Displays an Open Conformation

BY ROLF KARLSSON

Department of Medicine, 0654, *University of California, San Diego*, 9500 *Gilman Drive, La Jolla, CA* 92093-0654, *USA*

JIANHUA ZHENG

Department of Chemistry, 0654, *University of California, San Diego*, 9500 *Gilman Drive, La Jolla, CA* 92093, *USA*

NGUYEN-HUU XUONG

Departments of Biology, Physics and Chemistry, 0317, *University of California, San Diego*, 9500 *Gilman Drive, La Jolla, CA* 92093-0654, *USA*

SUSAN S. TAYLOR

Department of Chemistry, 0654, *University of California, San Diego*, 9500 *Gilman Drive, La Jolla, CA* 92093, *USA*

AND JANUSZ M. SOWADSKI*

Department of Medicine, University of California, San Diego, 9500 *Gilman Drive, La Jolla, CA* 92093-0654, *USA*

(*Received* 15 *January* 1993; *accepted* 2 *March* 1993)

Abstract

The crystal structure of a binary complex of the porcine heart catalytic (*C*) subunit of cAMP-dependent protein kinase (space group $P4_132$; a = 171.5 Å) complexed with a di-iodinated peptide inhibitor, PKI(5–24), has been solved and refined to 2.9 Å resolution with an overall R of 21.1%. The r.m.s. deviations from ideal bond lengths and angles are 0.022 Å and 4.3°. A single isotropic B of 17 Å^2 was used for all atoms. The structure solution was carried out initially by molecular replacement of electron density followed by refinement against atomic coordinates from orthorhombic crystals of a binary complex of the mouse recombinant enzyme previously described [Knighton, Zheng, Ten Eyck, Ashford, Xuong, Taylor & Sowadski (1991). *Science*, **253**, 407–414]. The most striking difference between the two crystal structures is a large displacement of the small lobe of the enzyme. In the cubic crystal, the β-sheet of the small lobe is rotated by 15° and translated by 1.9 Å with respect to the orthorhombic crystal. Possible explanations for why this binary complex crystallized in an open conformation in contrast to a similar binary complex of the recombinant enzyme are discussed. This study demonstrates that considerable information about parts of a crystal structure can be obtained without a complete crystal structure analysis. Specifically, the six rigid-group parameters of a poly-alanine model of the β-structure were obtained satisfactorily from a crystal structure by refinement of difference Fourier coefficients based on an approximate partial structure model.

Introduction

cAMP-dependent protein kinase (cAPK) is one of the simplest members of a large and diverse family of enzymes that are of fundamental importance for regulation in the eukaryotic cell (Taylor, Buechler & Yonemoto, 1990). Because all of these enzymes have apparently evolved, in part, from a common origin, this simple enzyme can serve as a prototype for the entire family (Hanks, Quinn & Hunter, 1988). cAPK, in its inactive holoenzyme form, is a tetramer composed of two regulatory (R) and two catalytic (C) subunits. The active form of the enzyme is the C-subunit monomer. It contains 350 amino acids (Shoji, Ericsson, Walsh, Fischer & Titani, 1983) and is one of the smallest protein kinases.

* To whom all correspondence should be addressed.

In trying to understand the mechanism by which protein kinases transfer the γ-phosphate of ATP to a protein substrate, it is important to understand the conformational changes that are induced by substrate binding. Circular dichroism provided the first indication of substrate-induced conformational changes in the *C* subunit (Reed & Kinzel, 1984). Low-angle neutron scattering subsequently demonstrated that the binding of substrates leads to a reduction in the radius of gyration (Parello & Timmins, personal communication). Two structures of the recombinant mouse catalytic (*C*) subunit of cAPK were solved previously. A binary complex containing a 20-residue inhibitor peptide derived from the heat-stable protein kinase inhibitor (PKI) provided the first description of any protein kinase (Knighton *et al.*, 1993; Knighton, Zheng, Ten Eyck, Ashford *et al.*, 1991). A ternary complex containing ATP and the inhibitor peptide (Zheng, Trafny *et al.*, 1993; Zheng, Knighton *et al.*, 1993) describes how multiple conserved residues converge at the active site to facilitate ATP binding and catalysis. Both of these structures represent a 'closed' conformation and are consistent with the low-angle neutron scattering. We report here the structure of the mammalian porcine *C* subunit co-crystallized with a 20-residue di-iodinated inhibitor peptide. This complex shows an 'open' conformation relative to the earlier structures. A preliminary comparison with the apoenzyme form and a ternary complex of the mammalian enzyme indicate that this binary complex resembles the apoenzyme structure and is distinct from the ternary complex.

Experimental procedures

The porcine heart *C* subunit* was purified as described previously (Nelson & Taylor, 1981). The inhibitor peptide, PKI(5–24), corresponds to the amino terminus of a heat-stable protein kinase inhibitor (PKI) (Cheng, van Patten, Smith & Walsh, 1986): TTYADFIASGRTGRRNAIHD. The peptide was synthesized by the La Jolla Cancer Research Foundation facility. This peptide was fully iodinated at Tyr7 and purified to homogeneity by high performance liquid chromotography.

The crystals, grown according to Knighton, Zheng, Ten Eyck, Ashford *et al.* (1991) using enzyme:inhibitor molar ratios of 1:6, belong to the cubic space group $P4_132$ with unit-cell dimension $a = 171.52$ Å (Table 1). For comparison the crystals obtained from the recombinant enzyme are also summarized in Table 1. Diffraction data were collected at 277 K with graphite-monochromated Cu $K\alpha$ X-rays from a Rigaku RU-200 rotating-anode diffractometer at the UCSD Research Resource equipped with two Xuong–Hamlin multiwire area detectors (Hamlin *et al.*, 1981; Xuong, Sullivan, Nielsen & Hamlin, 1985). Collecting 119 740 reflections resulted in 17 821 unique reflections to 2.9 Å resolution with an overall $R_{sym} = 9.7\%$ [$R_{sym} = (\sum|I_{obs} - I_{avg}|)/(\sum I_{avg})$].

Table 1. *Summary of crystal forms of porcine heart and recombinant mouse C subunits*

Enzyme	Apoenzyme	Binary complex	Ternary complex
Mammalian porcine	Cubic $P4_132$ $a = 169.24$ Å (Knighton, Xuong, Taylor & Sowadski, 1991)	Cubic $P4_132$ $a = 171.52$ Å	Hexagonal $P6_122$ $a = b = 80.16$, $c = 288.07$ Å (Knighton, Xuong, Taylor & Sowadski, 1991)
Recombinant mouse	No crystals obtained	Orthorhombic $P2_12_12_1$ $a = 73.62$, $b = 76.52$, $c = 80.14$ Å (Zheng *et al.*, 1992)	Orthorhombic $P2_12_12_1$ $a = 73.70$, $b = 76.26$, $c = 80.74$ Å (Zheng *et al.*, 1992)

Molecular replacement of electron density

Since this crystal form did not diffract to high angle, no native isomorphous data were collected for the cubic crystals. Instead, the molecule was related to the orthorhombic crystal structure (OCS) by the molecular-replacement method (MR), using a multi-solution approach to the two-stage procedure of Rossmann (Rossmann, 1990).

Since no atomic model was available at the time, the electron density of one binary complex of mouse recombinant *C* subunit isolated from the solvent-flattened single isomorphous replacement (SIR) electron-density map (Knighton, Zheng, Ten Eyck, Ashford *et al.*, 1991) was used as search model. The complex Fourier coefficients F_{model} of the search model at various orientations in the cubic cell were obtained by linear interpolation for use in calculations of the rotation and translation functions.

The overlap between the observed and one-molecular Patterson function (PF) was taken as a measure for the likelihood of the orientation of the density model (Rossmann & Blow, 1962). The overlap rotation function (RF) was evaluated as the sum $\sum_h |F_o|^2 |F_{model}|^2$ using the 500 largest observed Patterson coefficients $|F_o|^2$ in the resolution range 7.0–3.6 Å.

The Eulerian angular system was chosen with α, β and γ corresponding to the orthogonal rotation-axis

* The amino-acid sequence of the porcine heart *C* subunit differs from the amino-acid sequence of mouse recombinant *C* subunit at the following positions: Asn(Thr)32, Ala(Ser)34, His(Gln)39, Glu(Asp)44, Thr(Ser)65, Phe(Tyr)69, Tyr(Phe)108, Pro(Ala)124 and Ser(Thr)348, where the sequence of mouse enzyme is indicated in parentheses. In addition, the porcine heart *C* subunit, in contrast to the mouse recombinant *C* subunit, contains a myristic acid at its N-terminus.

sequence ZYZ. A step size of 4° in α and β and, in order to reduce the computations, a variable step size in γ of $4/\sin\beta$ ($\beta \neq 0$) resulted in 9449 independent angular combinations.

The molecular-position and space-group ambiguity was solved by the translation function (Crowther & Blow, 1967) using all data in the resolution range 7.0–3.6 Å. The translation functions corresponding to the seven independent Harker sections that are common to both space-group enantiomers, were calculated using the coefficients of the observed PF from which the origin had been removed. The seven translation functions were combined by the symmetry-sum function (SSF) (Pavelcik, 1989). The SSF gives the sum of the values at corresponding molecular vector positions in the seven translation functions as a measure for tentative molecular positions. Removal of the origin was accomplished by taking the difference between the observed and average Patterson coefficient in narrow interlacing shells of resolution. The correct orientation corresponded to the 230th largest RF peak (2.2σ), but the RF maximum was 4.4σ. The correct molecular position had an SSF value of 8.4σ, which was the largest value in all examined SSF functions. The next largest (false) maximum was 5.4σ.

The translational functions corresponding to the 16 independent Harker sections were combined by the SSF in order to solve the space-group ambiguity. A SSF maximum of 28.5σ was obtained for the correct enantiomer. The largest peak in each of the nine enantiomer-sensitive independent translation functions corresponded to a molecular Harker vector.

Refinement of the molecular-replacement solution

When the refined atomic coordinates of the OCS became available, the six parameters of the coordinate transformation were improved by minimizing the least-squares sum $\sum_h(|F_o| - |F_c|)^2$. All observed reflections in the resolution range 7–2.9 Å were used in this refinement and in all further calculations.

A difference Fourier synthesis showed that the phenyl ring of Tyr7 of the peptide inhibitor was iodinated at positions 3 and 5. An anomalous difference Fourier synthesis confirmed both iodine positions.

Molecular-replacement solutions of the hexagonal ternary and cubic apo-crystal structure

The hexagonal (OCS) and orthorhombic crystal structures were related by MR techniques using the previous electron-density search model and all data in the resolution range 7.0–3.5 Å. The relative orientation was given by the largest peak in the fast rotation function (Crowther, 1972). The translation functions corresponding the nine independent Harker sections combined by the SSF gave a peak of 31.7σ (with origin-removed Patterson coefficients) at the molecular position in the correct space group.

The six positional parameters were initially improved by the maximization of the overlap between the observed PF and the calculated PF of the electron-density model. Later Fourier coefficients of the large lobe were used based on the refined atomic parameters of the orthorhombic structure. The relative orientation, given in Eulerian angles, is $\alpha = 94.8$, $\beta = 89.85$ and $\gamma = 0°$ about the axis sequence ZYZ. This rotation brings the orthorhombic z axis parallel to the hexagonal x axis. Moreover, position (1/4, 0, 0) in the orthorhombic cell corresponds to position (0.000, 0.501, 0) in the hexagonal cell. Thus, the twofold screw axis parallel to the z axis in the orthorhombic cell will almost exactly coincide with the hexagonal crystallographic twofold screw axis (x, 1/2, 0) which performs the same operation as the twofold crystallographic x axis.

Since the orthorhombic c axis and hexagonal a axis are of equal length (80.2 Å) the lattice contacts between the two concerned equivalent molecules will be identical in the two crystal forms.

The crystal structure of the cubic apo form was intially related to the orthorhombic form using the electron-density model and the MR solution of the binary cubic form with data in the resolution range 8.0–3.9 Å.

The six positional parameters were improved as described for the hexagonal form. The C-subunit molecule was found to have almost identical orientation in both cubic crystal forms.

Clarification of conformational changes in the small lobe

Knighton, Zheng, Ten Eyck, Xuong *et al.* (1991) divided the molecule into two parts, the large lobe (residues 128–306 plus the peptide inhibitor) and the small lobe (residues 15–127 and 307–350). Inspection of various difference Fourier syntheses based on the MR solution suggested that the small lobe, or parts of it, might be displaced. The overlap between the observed and calculated PF was maximized by moving the small lobe interactively, while the large lobe was kept fixed. More accurate orientation and position of the large and small lobes was determined by the minimization of $\sum_h(|F_o| - |F_c|)^2$ using rigid-group refinement (Brünger, Kuriyan & Karplus, 1987). Rigid-group refinement lead to crystallographic R factors of 0.449 and 0.529 for the large lobe with no iodine and the small lobe, respectively. Refinement carried out for both lobes resulted in a

crystallographic R factor of 0.428 which was lowered ($R = 0.419$) if the I atoms were included.

A distinct difference, larger than would be expected based on molecular size alone, between the separate R values of the two lobes suggested that there are conformational differences between the small lobes of the two crystal forms. The small lobe was, in the next step, divided into six segments as follows: three helices A, B and C (residues 18–30, 76–83 and 84–97, respectively), the five-stranded β-sheet, and two interconnecting segments (residues 98–106 and 31–41) (see Table 2). These segments were reduced to poly-alanine and treated as rigid groups. The rigid-group parameters of each segment, initially given those of the globally adjusted small lobe, were refined separately by the minimization of the least-squares sum

$$Q_j = \sum_{hkl} |D - F_j|^2,$$

where D is the Sim-weighted difference Fourier coefficient set based on the large lobe alone, and F_j is the Fourier coefficient of peptide segment j. D is an estimate of the structure factor of the small lobe. F_j can be considered as a function of six rigid-group parameters measuring the deviation of segment j from the orthorhombic mouse recombinant C-subunit model placed according to the best fit of the large lobe in the cubic binary crystal structure. Noise reduction of the D values was attempted by refining the positional parameters of individual atoms of the large lobe to an R value of 38% using *TNT* (Tronrud, Ten Eyck & Mathews, 1987) with large weights on the geometrical restraints and then convoluting the D values by the Fourier transform of the molecular envelope at 8 Å resolution, in order to take advantage of the high solvent content. The volume fraction of the molecular mask, constructed to occupy all space within 2.5 Å of each tentative atom in the unit cell, is only 33%. The refined rigid-group parameters of the peptide segments are given in Table 3.*

Table 3 also contains the rigid-group parameters of the β-structure in the hexagonal structure (8–3.5 Å data) and the cubic apo structure (8–3.9 Å data). No refinement of individual atomic parameters of the large lobe had been undertaken, however, in the preparation of the D values. The refined parameters of the apo structure show the deviation from the refined cubic structure transferred to the apo structure.

Table 2. *Summary of α-helices and β-strands of the small lobe*

α-Helices	*A*	15–31
	B	76–82
	C	84–97
β-Strands	1	43–48
	2	57–63
	3	67–75
	4	106–111
	5	115–120

Table 3. *Refined rigid-group parameters of peptide segments of the small lobe with the average standard deviations (σ)*

The Eulerian angles α, β, γ (°) correspond to the orthogonal rotation-axis sequence ZYX and the shifts dx, dy, dz along the orthogonal axes XYZ, respectively, are given in Å. Table entries flagged as R show differences between the refined cubic crystal structure and the refined orthorhombic crystal structure. Those differences were obtained by minimization of Q in the resolution range 7–2.9 Å; however, the difference Fourier coefficient was replaced by the structure factor of the individual peptide segment at the refined cubic structure.

Segment	Flag	α	β	γ	$\langle\sigma\rangle$	dx	dy	dz	$\langle\sigma\rangle$
Beta	*R*	6.3	12.7	6.0	0.1	−2.2	1.6	0.8	0.01
Beta		6.2	11.9	6.0	0.5	−2.1	1.6	0.8	0.07
84–97	*R*	4.6	7.2	8.1	0.2	−0.6	1.1	−0.4	0.01
84–97		2.2	6.4	8.9	2.2	−0.6	1.1	−0.4	0.1
18–30	*R*	2.5	−0.8	1.0	0.1	0.4	−1.4	0.1	0.01
18–30		1.5	−0.4	0.2	2.0	0.4	−1.3	0.0	0.1
76–83	*R*	4.7	11.1	1.8	0.2	−2.8	3.2	−1.2	0.01
76–83		6.0	13.1	3.7	3.2	−2.8	3.2	−1.3	0.2
98–106	*R*	0.2	3.5	1.7	0.1	0.1	0.0	0.1	0.01
98–106		2.0	2.0	2.2	1.8	−0.1	0.0	0.2	0.1
31–41	*R*	4.3	6.6	5.9	0.1	−1.4	0.4	1.9	0.01
31–41		5.5	2.1	6.1	2.3	−1.3	0.5	1.9	0.2
Beta/hex		−0.7	0.4	−0.9	0.7	0.1	0.4	0.4	0.1
Beta/apo		1.6	1.4	−1.4	1.1	−0.9	−0.9	−0.1	0.1

Final refinement

The structure solution of the cubic binary complex proceeded with *TNT* refinement (initially with large weights on the geometrical restraints for bond distances and bond angles), difference Fourier techniques, and molecular modeling using the graphic display program *FRODO* (Jones, 1978). The R value is 21.1% for 2732 atoms and 17077 observed reflections in the resolution range 7–2.9 Å with a single overall temperature factor of 17.2 Å^2 and r.m.s. deviations from the ideal geometry of 0.022 Å for bond distances and 4.3° for bond angles. The optional solvent correction term in the *TNT* program was used with $K_{sol} = 0.84$ and $B_{sol} = 100$ Å^2. The relative weights on the geometrical restraints were 6.0 for bond distances and angles, 18.0 for trigonal atoms and planar groups, and 1.0 for contacts. The geometrical term of the least-squares sum was 3.0% of the X-ray term. A final refinement with fixed coordinates and individual temperature factors B

* Atomic coordinates and structure factors have been deposited with the Protein Data Bank, Brookhaven National Laboratory (Reference: 1CTP, R1CTPSF). Free copies may be obtained through The Technical Editor, International Union of Crystallography, 5 Abbey Square, Chester CH1 2HU, England (Supplementary Publication No. SUP 37079). At the request of the authors, the structure factors will remain privileged until 1 April 1994. A list of deposited data is given at the end of this issue.

constrained by the condition $B > 16$ Å^2 gave $R = 0.190$.

Residues 1–6, 318–326 and 339–340 of the main chain and the last two residues of the inhibitor could not be located with sufficient confidence and were omitted in the refinement. Residues 7–12, 331–338 and 341–342, which are poorly refined, and residues 327–330, which are stabilized by a crystal contact and thus rather well located, were included in the refinement. The poly-Glu sequence, 331–334, could be modelled in at least two ways, but only that model which made the most geometrical sense was refined. 44 residues were included in the refinement as alanine since their side chains could not be found. Most of these residues were charged and protruded into the solvent region. The first eight C atoms of the alkane tail of the myristylated N-terminal residue could be located even though the rest of the N terminus could not be located with confidence. A Ramachandran plot showed 12 non-glycine residues to be outside the allowed regions. In addition to regions discussed above these include residues 33, 35, 65, 242 and 286.

Discussion

The most important difference in this structure compared to the earlier structure of the recombinant *C*-subunit binary complex is the concerted motion of peptide segments in the small lobe. These two structures are superimposed in Fig. 1.

The dominant feature of the small lobe, shown in Fig. 1(*b*), is a β-sheet composed of five antiparallel strands. Three highly conserved features of this lobe are a glycine-rich loop between β-strands 1 and 2, Lys72 in β-strand 3, and Glu91 in the *C* helix which ion pairs with Lys72. The motion of the β-sheet can be formally described as a rotation of 15.0° about an axis that passes within 0.8 Å of at least one atom of residues 31, 103 and 315. The axis has a shift of 0.4 Å and is inclined 109° to an axis passing through the centre of gravity between the large and small lobes.

The motion of other parts of the small lobe are smaller and are coupled to the motion of the β-structure. The C-terminal portion of helix *C* is anchored to segment 98–106 which moves very little since it is fixed to the large lobe *via* hydrogen bonding involving residues Asn99, Phe102, Val104, Tyr156 and Val182. The N-terminal portion of helix *C*, however, follows the motion of helix *B* and rotates as much as 12°. This motion does not affect the important ion pairing between the conserved residues, Lys72 and Glu91, but does cause a change in the hydrogen bonding of His87 and Asn90. This change can be seen clearly in Fig. 2. The amide group of Asn90 shifts its hydrodgen bonding form O Glu86 in the OCS to O Ala188. In the OCS, His87 may form a weak link with His379 in the peptide; however, its most important contact is with the phosphate group of Thr197, which also forms a strong ionic interaction with Arg165. This phosphate group forms a 2.9 Å dimeric hydrogen bond to Arg165 in both crystals. Lys189 also ion pairs with Thr197 in both crystals. In the OCS, all groups that interact with the phosphate are derived from the large lobe with the exception of His87. In the cubic crystal, His87 moves 7 Å away from the phosphothreonine leaving the other interactions with the phosphate intact. The major contact between the small and large lobe in the cubic crystal in this region is through Asn90 and Ala188.

Helix *A* does not move much and is stabilized by the N-terminal myristyl group. For residues 31–41, the extended chain linking helix *A* with β-strand 1 moves 9°. Hydrogen bonds common to both structures link the backbones of Glu35 and Thr37 to that of Ser109 in β-strand 4.

Two structural segments, comprised of residues 31–97 and 107–120, form self-contained units. These segments have very few external hydrogen bonds that could prevent their concerted motion with the exception of the residues already mentioned, His87 and Asn90. Clearly these segments can move without disrupting any internal hydrogen bonds. Concerted motion of these segments opens and closes the bilobal cleft. Region 327–350 is uncertain and cannot be accounted for in this medium-resolution structure. This open conformational state is futher stabilized by crystal contacts, a detailed description of which will be presented elsewhere.

The conformation of the large lobe is very stable in comparison to the small lobe as a result of extensive hydrogen bonding between secondary structural elements within the lobe. Inhibitor binding also increases this stability. Deviations in conformation of the large lobe are of local character and relate to differences in crystal contacts and to the iodination of Tyr7, which causes the first two residues of the inhibitor to have a slightly different conformation.

The mammalian enzyme can assume either closed or open conformations based on the structures described here, and this is consistent with low-angle neutron scattering results (Parello & Timmins, personal communication). However, the binary complex formed with the iodinated PKI(5–24) and the mammalian enzyme adopts an open conformation similar, though not identical, to the apoenzyme. This is in contrast to the recombinant binary complex formed with the unmodified peptide. Several factors could account for the different conformations in the two binary complexes; however, the most likely explanation is that the iodination disrupts an important

crystal contact that is found in the hexagonal and orthorhombic crystals by changing the conformation of the first three residues of the peptide. Furthermore, the kinetics of mono- and di-iodinated peptide are identical to the unmodified peptide (Yap, 1984; Yap & Kemp, personal communication).

The equilibrium strongly favours the ternary complex when both APT and PKI are present (Whitehouse & Walsh, 1983). The appK_d for PKI(5–24) and the *C* subunit is 2 n*M* in the presence of ATP (Cheng *et al.*, 1986), but at least 2–3 orders of magnitude greater in the absence of MgATP (Herberg, Buechler & Taylor, 1993; van Patten, Fletcher & Walsh, 1986). Hence the equilibrium between the closed and open conformation is more reversible for the binary complex. Because the equilibrium between closed and open conformations does not strongly favour either, the structure may be more susceptible to packing constraints. Clearly the crystal-contact constraints as a result of the packing of the molecules are very similar in the hexagonal and orthorhombic crystal forms and very different for cubic crystal forms. Furthermore, the iodination would interfere with the contacts that are made between molecules in the hexagonal and orthorhombic crystals. Crystal packing may, therefore, favour the open conformation for the binary complex with the mammalian *C* subunit.

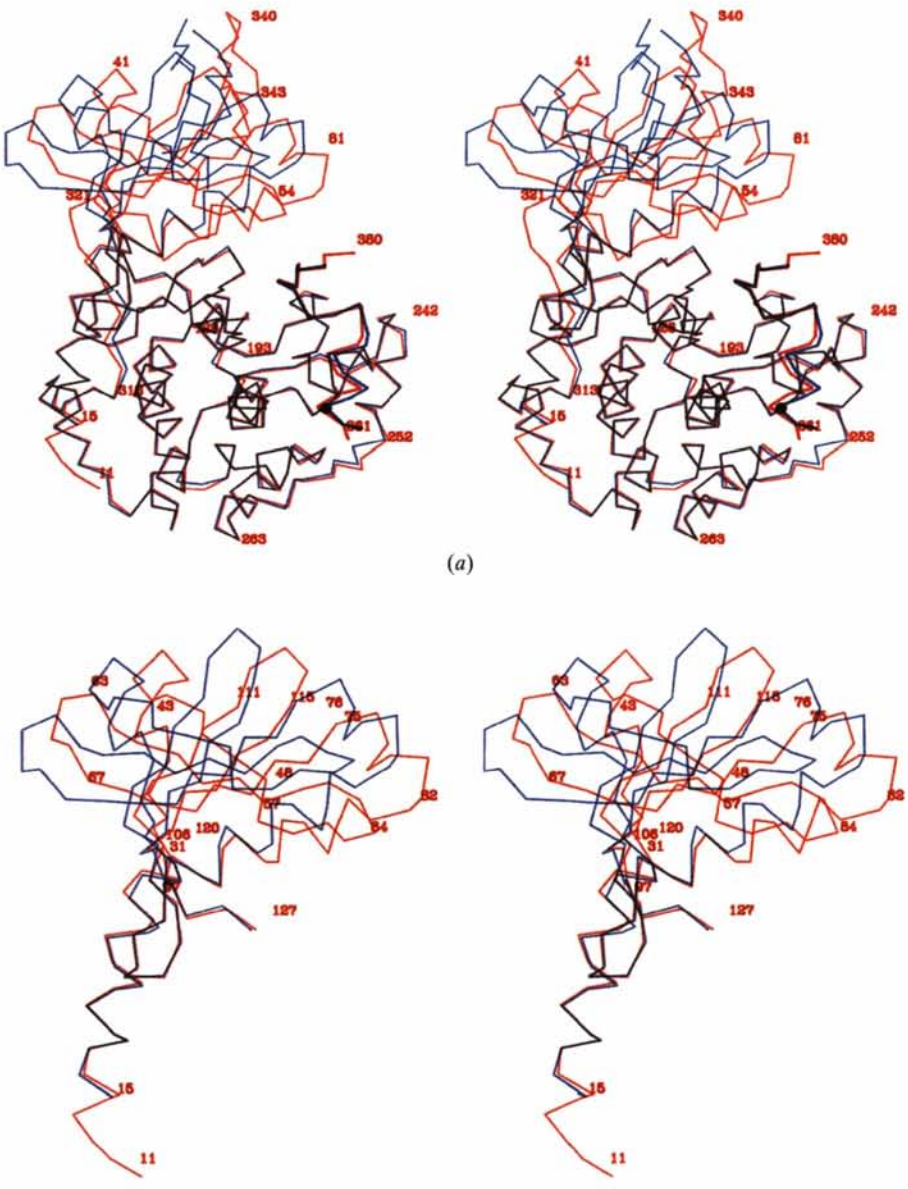

Fig. 1. Overall comparison of binary complexes of recombinant mouse and porcine heart *C* subunits. (*a*) Comparison of the C$^{\alpha}$ backbone traces of the porcine heart *C*-subunit binary complex (blue) with the mouse recombinant *C*-subunit binary complex (red). The coordinates for the mouse recombinant enzyme are from Knighton *et al.* (1993). The large lobes in these two structures are superimposed. Residues 128–300 and the inhibitor peptide constitute the large lobe and show an r.m.s. = 0.43. In contrast, large conformational changes are seen in the small lobe. These changes correlate with a rotation of the β-sheet. The C-terminal portion of the *C* subunit (residues 318–342) wraps around the small lobe and is well defined in the mouse recombinant *C* subunit, whereas in the porcine enzyme this segment is highly disordered and is, therefore, omitted from the C$^{\alpha}$ trace. Iodinated tyrosine of the inhibitor (indicated by the thicker trace) is marked by a dot. (*b*) Small lobe only with N- and C-termini of helices and β-strands marked by residue number.

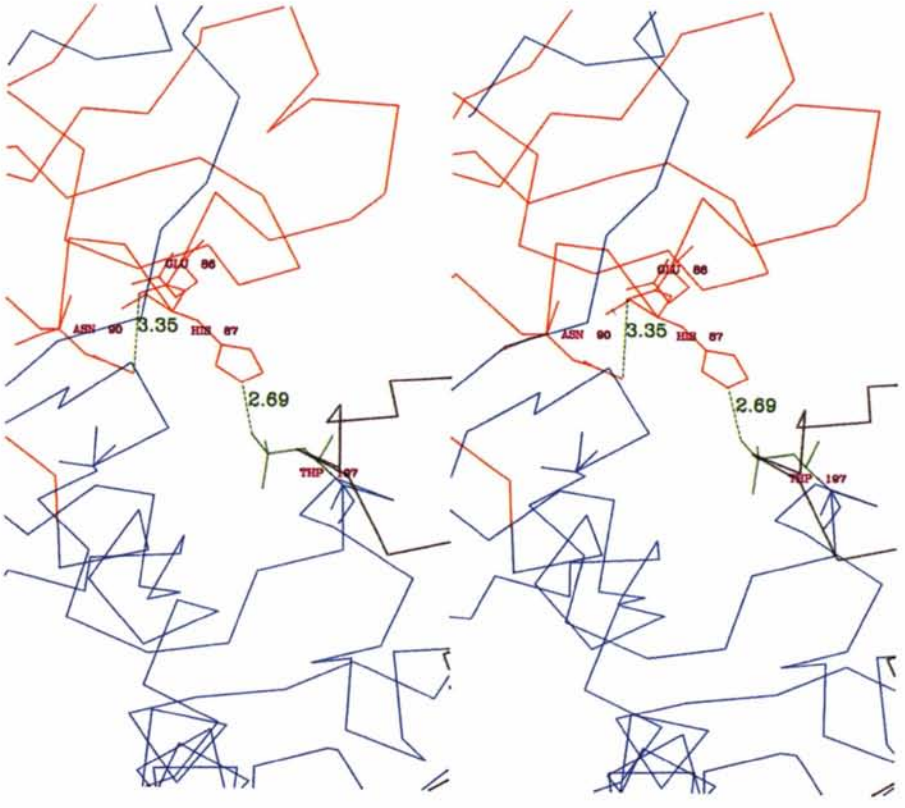

(*a*)

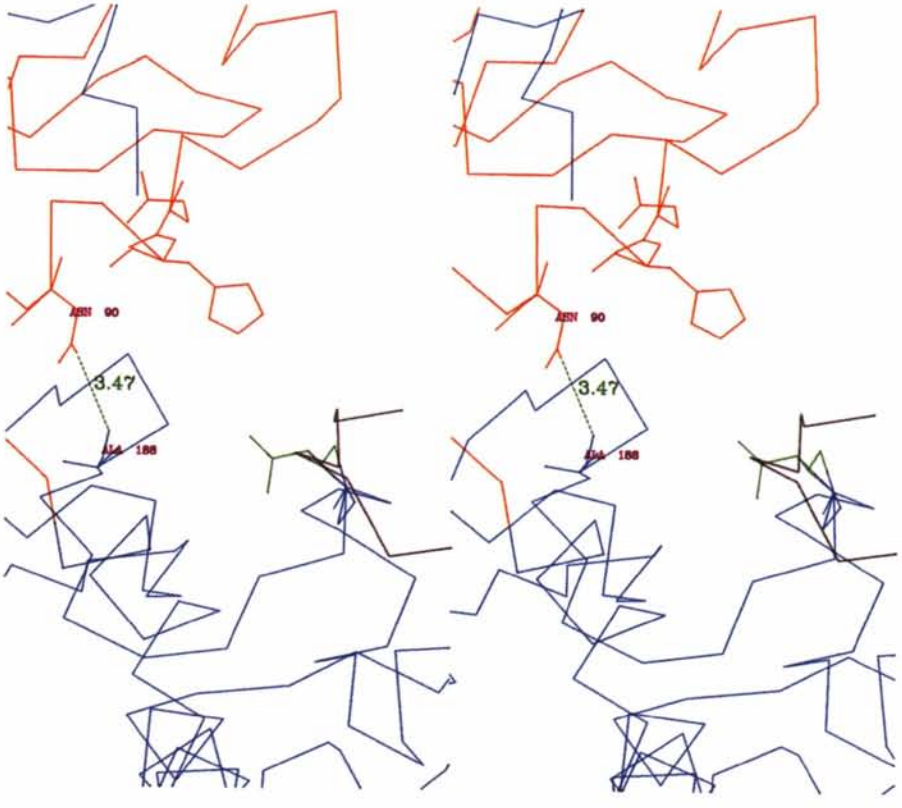

(*b*)

Fig. 2. Stereoview of the environment of His87. The small lobe is indicated in red and the large lobe in blue. The inhibitor is indicated in black. (*a*) In the recombinant mouse *C* subunit, His87 of the small lobe interacts with the stable phosphorylation site of Thr197 of the large lobe and the carbonyl group of the main chain of Glu86 interacts with the side chain of Asn90. (*b*) In the porcine heart *C* subunit, His87 moves away from the phosphate of Thr197 and the side chain of Asn90 of the small lobe interacts with the carbonyl of Ala188 of the large lobe. Distances are given in Å.

This work was supported in part by the Lucille P. Markey Charitable Trust without which this work could not have been completed, and by grants from NIH (SST, NX and JMS), the American Cancer Society (SST) and NSF (SST). We wish to thank Dr Lynn Ten Eyck for reviewing the manuscript. In addition, we thank Mr Gene Hasegawa for preparation of the manuscript, Mr David Appleby for preparation of the figures, and Mrs Siv Garrod for the purification of the iodinated peptide.

References

BRÜNGER, A. T., KURIYAN, J. & KARPLUS, M. (1987). *Science*, **235**, 458–460.

CHENG, H.-C., VAN PATTEN, S. M., SMITH, A. J. & WALSH, D. A. (1986). *Biochem. J.* **231**, 655–661.

CROWTHER, R. A. (1972). *The Molecular Replacement Method*, edited by M. G. ROSSMANN, pp. 173–178. New York: Gordon and Breach.

CROWTHER, R. A. & BLOW, D. (1967). *Acta Cryst.* **22**, 758–764.

HAMLIN, R., CORK, C., NIELSON, C., VERNON, W., MATTHEWS, D. & XUONG, N. (1981). *J. Appl. Cryst.* **14**, 85–93.

HANKS, S. K., QUINN, A. M. & HUNTER, T. (1988). *Science*, **241**, 42–52.

HERBERG, F. W., BUECHLER, Y. J. & TAYLOR, S. S. (1993). In preparation.

JONES, T. A. (1978). *J. Appl. Cryst.* **11**, 268–272.

KNIGHTON, D. R., BELL, S. M., ZHENG, J., TEN EYCK, L. F., XUONG, N., TAYLOR, S. S. & SOWADSKI, J. M. (1993). *Acta Cryst.* D**49**, 357–361.

KNIGHTON, D. R., XUONG, N., TAYLOR, S. S. & SOWADSKI, J. M. (1991). *J. Mol. Biol.* **220**, 217–220.

KNIGHTON, D. R., ZHENG, J., TEN EYCK, L. F., ASHFORD, V. A., XUONG, N., TAYLOR, S. S. & SOWADSKI, J. M. (1991). *Science*, **253**, 407–414.

KNIGHTON, D. R., ZHENG, J., TEN EYCK, L. F., XUONG, N., TAYLOR, S. S. & SOWADSKI, J. M. (1991). *Science*, **253**, 414–420.

NELSON, N. C. & TAYLOR, S. S. (1981). *J. Biol. Chem.* **256**, 3743–3750.

PATTEN, S. M. VAN, FLETCHER, W. H. & WALSH, D. A. (1986). *J. Biol. Chem.* **261**, 5514–5523.

PAVELCIK, F. (1989). *J. Appl. Cryst.* **22**, 181–182.

REED, J. & KINZEL, V. (1984). *Biochemistry*, **23**, 968–973.

ROSSMANN, M. G. (1990). *Acta Cryst.* A**46**, 73–82.

ROSSMANN, M. G. & BLOW, D. (1962). *Acta Cryst.* **15**, 24–31.

SHOJI, S., ERICSSON, L. H., WALSH, D. A., FISCHER, E. H. & TITANI, K. (1983). *Biochemistry*, **22**, 3702–3709.

TAYLOR, S. S., BUECHLER, J. A. & YONEMOTO, W. (1990). *Annu. Rev. Biochem.* **59**, 971–1005.

TRONRUD, D. E., TEN EYCK, L. F. & MATHEWS, B. W. (1987). *Acta Cryst.* A**43**, 489–501.

WHITEHOUSE, S. & WALSH, D. A. (1983). *J. Biol. Chem.* **258**, 3682–3692.

XUONG, N., SULLIVAN, D., NIELSEN, C. & HAMLIN, R. (1985). *Acta Cryst.* B**41**, 267–269.

YAP, B. (1984). MSc thesis, Univ. of Melbourne, Australia.

ZHENG, J., KNIGHTON, D. R., TEN EYCK, L. F., KARLSSON, R., XUONG, N., TAYLOR, S. S. & SOWADSKI, J. M. (1993). *Biochemistry*. In the press.

ZHENG, J., KNIGHTON, D. R., XUONG, N., PARELLO, J., TAYLOR, S. S. & SOWADSKI, J. M. (1992). *Acta Cryst.* B**48**, 241–244.

ZHENG, J., TRAFNY, E. A., KNIGHTON, D. R., XUONG, N., TAYLOR, S. S., TEN EYCK, L. F. & SOWADSKI, J. M. (1993). *Acta Cryst.* D**49**, 362–365.